المجلة العلمية لجامعة الملك فيصل
The Scientific Journal of King Faisal University
العلوم الأساسية والتطبيقية
Basic and Applied Sciences

Assessing Degree of Desertification Using Tasselled Cap Transformation and Spectral Indicators Techniques: Iraq

Reem Tuama Yousuf and Ebtihal T AL-Khakani
Department of Physics, College of Education for Girls, University of Kufa, Kufa, Iraq

تقييم درجات التصحر باستخدام تقنيات تحويل الغطاء الخضري والمؤشرات الطيفية: العراق

ريم طعمة يوسف و ابتهال تقي حسن
قسم الفيزياء، كلية التربية للبنات، جامعة الكوفة، الكوفة، العراق

KEYWORDS الكلمات المفتاحية
Remote sensing, desertification index, Landsat 8, albedo, modified soil-adjusted vegetation
استشعار عن بعد، لاندسات 8، مؤشر التصحر، البيدو، مؤشر الغطاء النباتي المعدل للتربة المعدل (MSAVI)

RECEIVED الاستقبال	ACCEPTED القبول	PUBLISHED النشر
02/09/2020	19/11/2020	01/06/2021

https://doi.org/10.37575/b/sci/0019

ABSTRACT

Remote sensing technology is an advanced approach for monitoring desertification by extracting a variety of spectral indicators derived from satellite images. This research aims to monitor and assess the degree of desertification in An-Najaf City using Landsat 8 Operational Land Imager (OLI) images obtained on 7 August 2019. Three tasselled cap transformation (TCT) indices were employed: tasselled cap brightness (TCB), tasselled cap greenness (TCG), and tasselled cap wetness (TCW), in addition to the modified soil adjusted vegetation index (MSAVI), topsoil grain size index (GSI), and land surface albedo (albedo). Linear regression was performed on TCB-TCG, TCB-TCW, albedo-MSAVI, and GSI-MSAVI to select the group with the highest negative correlation. The two highest negative correlations were for the TCB-TCW model of coefficient r2=0.8894 and TCB-TCG of r2=0.8519. Based on these two models, the extracted degree of desertification index (DDI) showed a high overall accuracy of 88.14% for the TCB-TCW model, and 91.44% for the TCB-TCG model. The results of these two models demonstrate their effectiveness in evaluating the degree of desertification. In general, this study provides a simple, easy and effective method to monitor desertification levels in semi-arid lands.

الملخص

تعد تكنولوجيا الاستشعار عن بعد نهجًا متقدمًا لرصد التصحر عن بُعد من خلال استخراج العديد من المؤشرات الطيفية المستمدة من مرئيات الأقمار الصناعية. يهدف هذا البحث إلى مراقبة مستويات التصحر وتقييمها في محافظة النجف باستعمال مرئيات لاندسات OLI 8 (تصوير الأراضي التشغيلية) التي تم الحصول عليها في 7 أغسطس 2019. في هذه الدراسة، تم استعمال ثلاث من مؤشرات تحويل الغطاء الخضري (TCT)، مؤشر السطوع (TCB)، ومؤشر الاخضرار (TCG)، ومؤشر الرطوبة (TCW)، فضلاً عن بعض المؤشرات الطيفية كمؤشر الغطاء النباتي المعدل للتربة المعدل (MSAVI)، ومؤشر حجم حبوب التربة السطحية (GSI) وبياض سطح الأرض (الالبيدو). تم إجراء الانحدار الخطي على المجاميع TCB-TCG و TCB-TCW و GSI-MSAVI و albedo-MSAVI لاختيار مجموعة الارتباط السلبي الأعلى، وظهر أن أعلى ارتباطين سلبيين بين TCB-TCW بمعامل تحديد (= r2 0.8894) و TCB-TCG مع (0.8519 = r2). بناءً على هذين النموذجين، أظهر مؤشر درجة التصحر المستخرج (DDI) دقة إجمالية عالية بلغت 88.14% لنموذج TCB-TCW و 91.44% لنموذج TCB-TCG. أثبتت نتائج هذين النموذجين فعاليتهما في تقييم درجة التصحر، كما وان هذه الدراسة بعامة، وفرت طريقة فعالة وبسيطة وسهلة التطبيق لرصد مستويات التصحر في الأراضي القاحلة وشبه القاحلة.

1. Introduction

The desertification phenomenon is considered the most important global environmental problem as it influences more than 250 million people worldwide (Guo et al., 2017:1). The United Nations Convention to Combat Desertification (UNCCD: 1994) defines desertification as the degradation of soil and a biologically productive land system in arid and semiarid regions, resulting from several factors including climate change (reduced precipitation and high temperatures) and human activity (population density, erroneous land management, etc.). Desertification is described foremost by its impact on vegetation and soil (An et al., 2019:1). The causes and effects of desertification relate to many interdependent human activities that directly affect many of the Earth's resources (soil, water and vegetation) and include a variety of economic sectors, social groups and institutions (Briassoulis, 2019:2). An-Najaf City is characterised by a dry climate caused by a lack of and fluctuation in precipitation levels. High summer temperatures and a high degree of evaporation contribute to changes in land surface conditions, such as low vegetation and biomass, in addition to changes in soil properties, which lead to a degradation of the ecosystem (Lamqadem et al., 2018:2). To varying degrees, changes in the Earth's surface conditions make the spectral characteristics of desertified lands look different. This can be monitored by satellite sensors. This is necessary in order to assess desertification through spectral indicators derived from satellite data, which has proven effective for distinctive land degradation indicators (Xu et al., 2009:2). With the rapid progress of remote sensing technology in recent decades by way of integration with the Geographical Information System (GIS), the applications for remote sensing technology in desertification monitoring have also evolved (Al-khakani et al., 2018:573). Compared with field-based studies, which are the traditional methods for assessing land desertification, assessment based on remote sensing is a cost-effective and less time-consuming way to map land degradation risk (Lamqadem et al., b2018:2). The tasselled cap transformation (TCT) has been used in map making and to assess vegetation status and land degradation changes that are revealed by different satellites (Samarawickrama et al., 2017:13). The term 'tasselled cap' was given to decipher the shape developed after the graphic distribution of sketched data (Kauth and Thomas, 1976:1). The TCT tool may be used to distinguish regions where desertification appears. In general, three factors are used in TCT-based analysis: brightness, greenness, and wetness. These are usually called TCT components (Lamqadem et al., a2018:2). Sand areas and bare soil are highly reflective; therefore, these topographic features can be well-observed using a brightness component. The greenness component is used in monitoring healthy vegetation regions, and the wetness component is suitable for observing humid areas (Balcik and Ergene, 2016:254).

Many researchers have studied desertification assessment using spectral indicator techniques, for example Rocio et al. (2016). They created the degree of desertification index (DDI) model based on the NDVI-α feature space in the state of Querétaro on the central Mexican plateau. However, Mfondoum et al. (2016) assessed the land degradation status in the far north of Cameroon in Central Africa using the relationship of MSAVI2 and NDBSI, NDTeI, GSI, CI, NDSDI, and $SPC1_{R\text{-}NIR\text{-}SWIR1\text{-}SWIR2}$ indices. Similarly, Wei et al. (2018) applied albedo-NDVI, albedo-MSAVI and albedo-TGSI feature space models to extract desertification information on the Mongolian plateau. Atman et al. (2018) used the combination of albedo-NDVI, TCG-TCB and TCW-TCB to map the degree of desertification in the middle of the Draa Valley in Morocco. The results showed that the best performance was for the TCW-TCB model. Wu et al. (2019) utilised a desertification index (SASDI) model in the Shengli area of Inner Mongolia depending on albedo-MSAVI feature space to analyze the impact of desertification on the biophysical properties of the soil.

Corresponding Author: Ebtihal T AL-Khakani ibtihal.alkhaqani@uokufa.edu.iq , 0096407829785431 المؤلف المراسل: ابتهال تقي حسن

In this work, spectral indicators such as TCT_S, MSAVI, GSI and albedo have been used to assess the degree of desertification depending on the result of regression analyses of the GSI-MSAVI, albedo-MSAVI, TCB-TCG and TCB-TCW models.

The goals of this research are: 1) invert the TCT_S, MSAVI, GSI and albedo data using remote sensing images to assess the hazard of desertification by analysing the correlation of spectral indicators; and 2) map the degree of desertification in the studied area according to the results of the negative regression analysis.

This research is one of only a few that have adopted remote sensing techniques to evaluate desertification in An-Najaf City. Therefore, it is expected to be a good reference for the traditional methods that have previously been utilised for dynamic observation of desertification in the studied zone.

2. Materials

2.1. Study Location:

Due to the dry climate, water scarcity and soil erosion, most areas of An-Najaf City face ecological deterioration. Therefore, An-Najaf City has been chosen as the study region for this research. An-Najaf Province lies 160 km south of the capital city of Baghdad, at a height of 70 m above sea level and with an area of about 28,824 km^2. The climate is hot and dry in summer with a temperature of more than 50°C, and cold and moderately rainy in winter with temperatures ranging from 1–10°C. The rainy season runs from October to April with an annual rainfall average of about 80 mm (AL-Khakani and Yousif, 2019:2).

The study region represents the northeastern part of An-Najaf Province (Figure 1), with an area of nearly 1,288.9 km^2 ranging between latitude 31° 45′–32° 19′ N and longitude 44° 8′–44° 45′ E. The land cover of the selected zone is represented by bare land, urbanised areas, desert and agricultural fields.

Figure 1. (A) An-Najaf Province in Iraq, (B) study location in An-Najaf Province, (C) study area

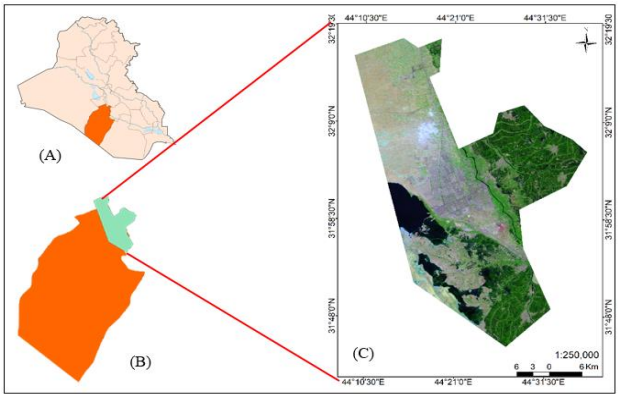

2.2 Data Sources and Pre-processing:

The desertification process in the selected area was assessed utilising Landsat 8 OLI sensor images (path/row 168/38) acquired on 7 August 2019 in the midst of the dry season when there is no rain and the vitality of chlorophyll is very slow; hence, there is a decrease in agricultural activities. The image, downloaded from http://landsat.usgs.gov, was cloud-free. It has been geo-corrected to a Universal Transverse Mercator (UTM) coordinate system via the World Geodetic System (WGS) 1984 datum, Zone 38. Because the research relies on spectral indicators which are linked to the biophysical aspects of desertification processes, the digital number of Landsat 8 OLI band values has been transformed to top of atmosphere (TOA) reflectance according to the methods provided by the user handbook for the Landsat 8 data. Landsat 8 surface reflectance images do not require additional radiometric or atmospheric corrections. ArcGIS 10.5 software was utilised for pre-processing and Excel 2019 was used to achieve the correlation analysis.

3. Methodology

In this paper, the proposed methodology relies on analysis of the relationship between various biophysical spectral indicators and the degree of desertification. The object of this method is to adopt the best group of spectral indicators to reveal the strongest negative correlation. The research methodology includes three major steps:

(1) Pre-processing of Landsat 8 imagery followed by calculation of spectral indices and TCT bands; (2) implementation of linear regression analysis on several groups of spectral indicators; and (3) development and application of an index for distinguishing the different levels of desertification in the study area.

3.1. Calculation of Spectral Indices:

Spectral indicators have shown their ability to detect land degradation. In general, the use of remote sensing to monitor and evaluate land degradation is linked to the spectral reflectance of vegetation and soil (Al-Bakri et al., 2012:1). In this work, some spectral indicators have been applied:

3.1.1. Modified Soil Adjusted Vegetation Index (MSAVI)

The vegetation index is a significant factor in evaluating the productivity of soil via the derived information about vegetation cover (Cui et al., 2011:110). Among these indicators, several studies have revealed that MSAVI is beneficial because it enhances the dynamic domain of the vegetation signal while reducing the effect of background soil (Guo et al., 2017:4). As a result, it is used to detect areas with low vegetation coverage according to the formula (Cui et al., 2011:112):

$$MSAVI = \frac{2\rho_{NIR}+1-\sqrt{(2\rho_{NIR}+1)^2-8(\rho_{NIR}-\rho_{RED})}}{2} \quad ...(1)$$

Where, ρ_{NIR} and ρ_{RED} are the reflectance values in the near-infrared and red bands of Landsat 8 OLI images, respectively.

3.1.2. Topsoil Grain Size Index (GSI)

Topsoil texture is closely associated with land degradation. Different levels of desertification have a mixed topsoil texture; the more intense the desertification, the coarser the topsoil (Xiao et al., 2006:2412). The value of GSI is near 0 or a smaller value in cultivated zones, and it is a negative value for bodies of water, whereas higher positive values of GSI appear to be areas influenced by sands, i.e., desert. The mathematical formula for the GSI index is (Pandey et al., 2013:6):

$$GSI = \frac{\rho_{RED}-\rho_{BLUE}}{\rho_{RED}+\rho_{GREEN}+\rho_{BLUE}} \quad ...(2)$$

3.1.3. Albedo

Albedo is a spectral characteristic of the earth's surface defined as the instantaneous proportion of reflected solar radiation from the target to the flow of incident radiation through the short-wave spectral range (Wu et al., 2019:4). It is an important index for determining the alteration of surface conditions such as aridity/humidity and temperature, which can cause desertification (Lamqadem et al., a2018). Generally, replacing vegetation cover with bare soil results in an increase of land surface albedo, which implies a degradation in the quality of land (Guo et al., 2017:5). In this paper, broad-band albedo has been adopted, which is specified by the collection of narrow-band albedos for each Landsat 8 band using the formula established by Liang (2001):

$$\text{Albedo OLI} = 0.356\rho_2+0.130\rho_4+0.373\rho_5+0.085\rho_6+0.072\rho_7-0.0018 \quad (3),$$

where albedo-OLI characterises the broad-band albedo of Landsat OLI

and ρ is narrow-band albedo for each band of Landsat OLI.

3.2. Tasselled Cap Transformation:

TCT is a useful method to compress the spectral data into a few bands linked to physical scene characteristics. It was introduced in 1976 by Kauth and Thomas utilising Landsat-5 MSS (Huang et al., 2002:1741). The concept of TCT is the linear transformation across a group of coefficients of pixel values in original bands (usually highly correlative) to a new group of bands that are orthonormal. New bands clarify the features and have been developed to relate to different types of land cover (Zanchetta and Bitelli, 2017:4). The TCT of Landsat TM or ETM+ comprises six multispectral features, and the first three bands are used often (Li and Chen, 2014:141). The first TC band matches the total brightness of the scene. The second TC band matches greenness and is usually employed as an indicator of the density of vegetation coverage. The third TC band is used as an index for the wetness of soil (Lamqadem et al., a2018:6). TCT does not depend on the image and may be applied to different images, provided that the transactions for this type of satellite are calculated. As a result, it needs a set of coefficients which weigh the multispectral image bands, where the sum gives a new value (Li et al., 2016:2). Table 1 presents the coefficients of transformation employed in this research for Landsat 8 OLI to get the TCT indicators. The mathematical models for brightness, greenness and wetness have been calculated according to Formulas 4, 5 and 6 (Crist and Kauth 1986: 84):

Brightness=$0.3037\rho_2+0.3608\rho_3+0.3564\rho_4+0.7084\rho_5+0.2358\rho_6+0.1691\rho_7$...(4)

Greenness=$-0.3064\rho_2-0.3300\rho_3-0.4325\rho_4+0.6860\rho_5-0.0383\rho_6-0.2674\rho_7$.... (5)

Wetness=$0.2097\rho_2+0.2038\rho_3+0.1017\rho_4+0.0685\rho_5-0.7460\rho_6-0.5548\rho_7$.... (6)

Table 1. Tasseled Cap Component Coefficients for Landsat 8 OLI Images (Li et al., 2016:8)

TCT	Blue	Green	Red	NIR	SWIR1	SWIR2
Brightness	0.3037	0.3608	0.3564	0.7084	0.2358	0.1691
Greenness	-0.3064	-0.3300	-0.4325	0.6860	-0.0383	-0.2674
Wetness	0.2097	0.2038	0.1017	0.0685	-0.7460	-0.5548

3.3. Determination of the Degree of Desertification (DDI):

Any two indicators are deemed equivalent if it is possible to take a decision based on one indicator equally well as on the other indicator (Perry and Lautenschlager, 1984:2). Furthermore, the binary distinction between types of vegetation cover and non-vegetation is required for at least one pair of indicators to ensure that these two types of ground cover are separated in the feature area (Baraldi et al., 2006:2577). In the description of land degradation, the indicators were grouped into five pairs according to their relationship.

The linear regression model has been performed to compare and choose the group offering the highest negative correlation. About 500 points were randomly chosen utilising the GIS tools for the entire study area. The values of albedo, MSAVI, GSI, TCB, TCW and TCG corresponding to each point were extracted to perform the correlation analysis for the four pairs. From albedo-MSAVI (first set), GSI-MSAVI (second set), TCB-TCW (third set) and TCB-TCG (fourth set), the groups with the highest negative correlation were chosen. Depending on these groups, the degree of desertification index equation has been applied. Based on the results presented by Verstraete and Pinty (1996), various desertification regions can be efficiently detached by segmenting the albedo-NDVI feature space in the perpendicular direction into changing orientations of desertification.

The perpendicular direction position in the albedo-NDVI feature space can be well-matched using a simple linear polynomial formula as follows:

DDI = K × NDVI-albedo ... (7)

Where DDI is the degree of desertification indicator and K is assigned by the slope of the suitable linear regression equation in the feature space (where k = -1/slope). According to the conclusions presented by Ma et al. (2011), the values of the DDI can be segmented into five different classes of desertification: non-desertification, low, moderate, high and severe, utilising Jenks' natural break classification, where the break points between classes are determined according to the nature of the data and its inherent groups. This algorithm maximises the difference between the classes while the internal variance for each class is at a minimum (Wei et al., 2018:6). This algorithm has been applied in many studies (Becerril-Pina et al., 2016; Lamqadem et al., a2018; Ma et al., 2011; Wei et al., 2018) to distinguish degrees of desertification depending on a variety of spectral indices, where it has offered higher precision than the training models or statistical data. In this paper, the DDI formula (Formula 7) will be applied according to the results of the strongest correlation between the different indicators used.

3.4. Accuracy Assessment:

To check the precision of the models, 200 verification points were randomly chosen from the study area. Then, the verification points were visually interpreted according to sentinel-2 satellite data and a Google Earth map. The ground-truth points were collected from diverse classes of the study region (i.e., dense vegetation cover, sparse vegetation, bare soil and wetland). To evaluate the accuracy of the final desertification maps, the confusion matrix and some statistical descriptors derived from this matrix, such as user accuracy, producer accuracy, overall accuracy and Kappa coefficient, were applied.

4. Results

4.1. MSAVI, GSI, Albedo, and TCT Indicators:

Figures 2 (a) and (b) show the results of applying the spectral indices of MSAVI, GSI, albedo, TCB, TCG and TCW. The high values of the MSAVI and TCG bands reached 0.672 and 0.312 respectively, representing the agricultural fields and palm orchards, while the lower values were -0.212 and -0.229, respectively, corresponding to the bodies of water and wetlands in the study area.

Figure 2 (a). From left to right, MSAVI, GSI and albedo

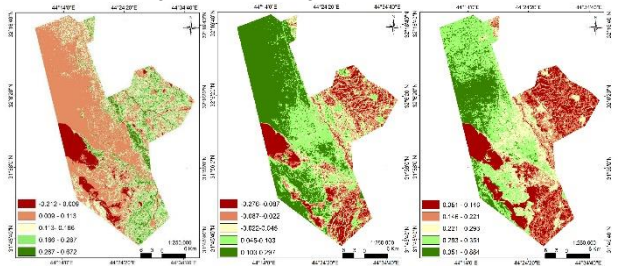

The high values of the GSI, TCB and albedo bands indicate drylands including sand dunes and fallow lands, and the low values refer to vegetation cover and bodies of water. TCW values ranged from -1.291 to 0.284, where the high values correspond to bodies of water, dense vegetation and wetlands, while the low values represent sand dunes and bare soil that is free of vegetation cover.

Figure 2 (b). Tasselled cap transformation indicators, from left to right: brightness, greenness and wetness

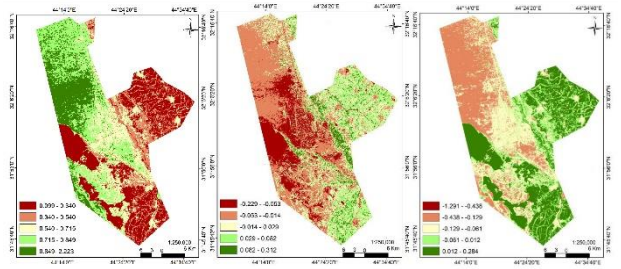

4.2. Results of a Linear Regression Analysis:

Results of the linear regression analysis for the four sets (Figure 3) showed that the negative correlations between MSAVI and each of GSI and albedo were slight with correlation coefficients of 0.483 and 0.3516, respectively, while a high negative relationship was found between TCB and TCW with r^2 =0.8894 and between TCB and TCG with r^2 =0.8519 at $p < 0.0001$. Therefore, the two groups, TCB-TCW and TCB-TCG, were selected to map the two models of degree of desertification. The regression equation for TCB-TCW and TCB-TCG models can be formulated according to two equations:

TCB = -2.8708 * TCW + 0.4065 ...(8)
TCB = -3.9884 * TCG + 0.6849 ...(9)

Based on the results of linear regression analysis, two new formulas have been suggested for extracting the DDI depending on the relationship of TCB-TCW and TCB-TCG, as follows

DDI = K * TCW-TCB ...(10)

DDI = K * TCG-TCB ...(11)

K values were assigned by slope for each of the two Equations 8 and 9. In this study, they were 0.3483 (1/2.8708 Equation 8) and 0.2507 (1/3.9884 Equation 9) respectively. Table 2 shows the ranges of the DDI values, areas and percentage of coverage for several desertification categories, which differed according to the two TCW-TCB and TCG-TCB models.

Figure 3. Correlation analysis of variables of different feature spaces for TCB-TCW, TCB-TCG, albedo-MSAVI and GSI-MSAVI

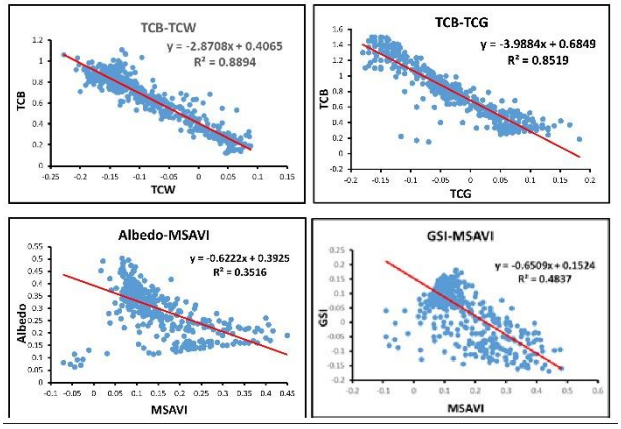

Table 2. Ranges of DDI values, areas and percentage of coverage for land at different levels of desertification for TCB-TCW and TCB-TCG models

Model	Degree of Desertification	DDI Range	Area (Km²)	% of Coverage
TCB-TCW	Severe desertification	< -0.33	338.809	26.29
	High desertification	-0.33 to -0.26	249.845	19.38
	Medium desertification	-0.26 to -0.18	192.839	14.96
	Low desertification	-0.18 to -0.10	199.321	15.46
	Non- desertification	> -0.10	308.173	23.90
TCB-TCG	Severe desertification	< -0.23	246.278	19.11
	High desertification	-0.23 to -0.19	285.477	22.15
	Medium desertification	-0.19 to -0.14	187.404	14.54
	Low desertification	-0.14 to -0.09	184.768	14.34
	Non- desertification	> -0.09	384.960	29.87

It is clear that the values of K and the extent of DDI values in the different desertification regions vary for the two feature-space patterns. In the severe desertification zones, the highest brightness values correspond to the lowest wetness values, which are often free of vegetation cover, while the non-desertified region has the highest vegetation cover, highest wetness and lowest brightness values.

4.3. Accuracy Assessment of the Degree of Desertification Results:

Table 3 shows the specific classification accuracy of the TCB-TCW and TCB-TCG models. The results show that the overall accuracy of classification of the TCB-TCG model attained 91.44% with a Kappa coefficient of 89.23, while the overall accuracy of the TCB-TCW model reached 88.14% with a Kappa coefficient of 85.11.

The producer and user accuracy of each class extracted by the TCB-TCW model were 100% and 84.61% for severe desertification, 86.46% and 92.50% for high desertification, 88.37% and 86.36% for moderate desertification, 80.43% and 90.24% for low desertification and 89.65% and 86.66% for non-desertification, respectively.

The producer and user accuracy of each class extracted by the TCB-TCG model were, respectively, 93.75% and 96.77% for severe desertification, 94.28% and 91.77% for high desertification, 92.10% and 92.10% for moderate desertification, 87.87% and 82.85% for low desertification and 89.79% and 93.61% for non-desertification.

Table 3 .Accuracy classification for the degree of desertification map of TCB-TCG and TCB-TCW models

Model	*Level*	*Producer Accuracy (%)*	*User Accuracy (%)*
TCB-TCW	Severe	100.00	84.61
	High	86.46	92.50
	Moderate	88.37	86.36
	Low	80.43	90.24
	Non	89.65	86.66
Overall Accuracy 88.14%			
Kappa Coefficient 85.11%			
Model	*Level*	*Producer Accuracy (%)*	*User Accuracy (%)*
TCB-TCG	Severe	93.75	96.77
	High	94.28	91.77
	Moderate	92.10	92.10
	Low	87.87	82.85
	Non	89.79	93.61
Overall Accuracy 91.44%			
Kappa Coefficient 89.23%			

It is generally noted that the two models recommended in this paper have comparatively high classification accuracy. Finally, the research results confirm that the relationship between vegetation density and soil brightness is an appropriate and effective tool in the quantitative assessment of desertification.

5. Discussion

Nowadays, several methods are used to monitor desertification by remote sensing, including regression model (Jingfeng et al., 2005), supervised classification (Wang et al., 2006), spectral mixture analysis (Röder et al., 2008), visual interpretation (Guangyin et al., 2015) and vegetation index (Xu et al., 2018). In this study, the advantage of the applied feature-space models technique, which depends on various spectral indicators, further improves the accuracy of desertification information at several levels when compared with the aforementioned methods.

The results of the linear regression analysis of the two models, MSAVI-GSI and MSAVI-albedo, show a slight negative relationship between MSAVI and the albedo and GSI indicators. The lowest negative correlation was between MSAVI and albedo. Therefore, these two models cannot be adopted/used in mapping desertification levels.

To get the relative relationship of soil brightness, vegetation and bodies of water in the process of desertification, TCT was successfully used to recuperate the indicators of TCB, TCG and TCW for brightness, vegetation coverage and soil wetness, respectively. Based on the correlation analysis of the TCT indicators, two degrees of desertification models were established in the TCW-TCB and TCG-TCB feature space to assign a map of the varying degrees of desertification for the studied area.

Although the TCW indicator reveals humid areas, whether bodies of water or dense vegetation cover, the TCB-TCW model excellently reveals the extreme contrast between dry soils and wet areas. Thus, TCB-TCW analysis results show a strong negative correlation (r^2=0.8894). This is consistent with the outcomes of Crist et al. (1986) and Lamqadem et al. (2018:a) who concluded that TCW can be closely related to soil and plant management. In this paper, TCB-TCW analysis confirms the efficiency of using TCW as an indicator for assessing the environment and vegetation in dry and semiarid regions.

The TCG-TCB model proposed in this study reveals a clear contrast between dry soil and vegetation areas. With aggravation from desertification, vegetation cover will decrease in addition to changing the surface energy balance and water, thereby reducing soil moisture and increasing surface whiteness (Wu et al., 2019:10). Therefore, the surface characteristics of the desertification process can directly influence the TCG-TCB feature space. Accordingly, the results also show that TCG has a high negative correlation with TCB ($r^2 = 0.8519$), indicating that the TCG indicator can be used efficiently in environmental monitoring and land cover assessment.

Figure 4 (a) shows a map of the degree of desertification based on the TCW-TCB model. According to this model, total percentage of desertification is around 76.09% of the entire area, whereas severe desertification is about 26.29%. High desertification is shown to be around 19.38%, while moderate desertification was limited to 14.96% and low desertification to 15.46%. Finally, the rate of non-desertification is 23.90% of the total area (see Table 2).

Based on the TCG-TCB model, an extracted map of the degree of desertification is illustrated in Figure 4 (b). As the map shows, the percentage of desertification is slightly lower than that obtained from the TCW-TCB model. In Table 2, the percentage of the desertified zone obtained from the TCG-TCB model has decreased to 70.13% of the entire area, which increases the non-desertified area to 29.87%. The percentages of the severe and high desertification are 19.11% and 22.15% respectively, and the percentages of moderate and low desertification are 14.54% and 14.34%.

Figure 4. Degree of desertification map results of two models: (a) TCB-TCW, and (b) TCB-TCG

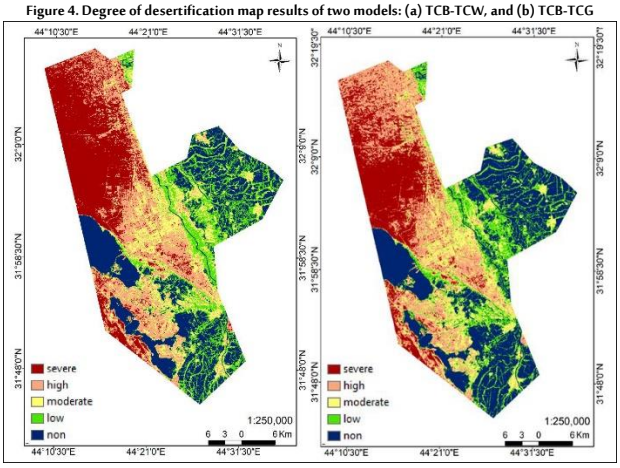

(a) (b)

In general, it is noticeable that the non-desertification lands are distributed along the southeastern region (seasonal crops, palm trees and fruits) and part of the western region (bodies of water) for the studied district, while the severe desertification areas are in the western region (sand dune creep areas) and small parts of the southwest (fallow lands).

Desertification studies often rely on extracting desertification information by interpreting land cover types in terms of patterns of vegetation cover and bare soil (Perry and Lautenschlager, 1984:11). Therefore, the results of the TCB-TCW and TCG-TCW models have been visually compared with the land cover classification map of the studied zone, as shown in Figure 5. According to the land cover classification map, the desertification area accounts for 70.66% of the total area, which is compatible with the research results.

The poor sensitivity of the TCB-TCW model with respect to the low-quality vegetation cover leads to interference between vegetation and barren soils in some areas. Therefore, the percentage of severe and low desertification lands appears higher than their value in the land cover classification map.

While the high sensitivity to vegetation cover of the TCB-TCG model increases the low desertification areas compared with the land cover classification map, by comparing the TCB-TCW and TCB-TCG models with the ground cover classification, it is clear that both models match the ground cover classification regardless of a slight decrease in the highly desertified area with the TCB-TCW model, while the TCB-TCG model showed a slight increase in high-desertified area and a slight decrease in low-desertified area.

Figure 5. Land cover classification map

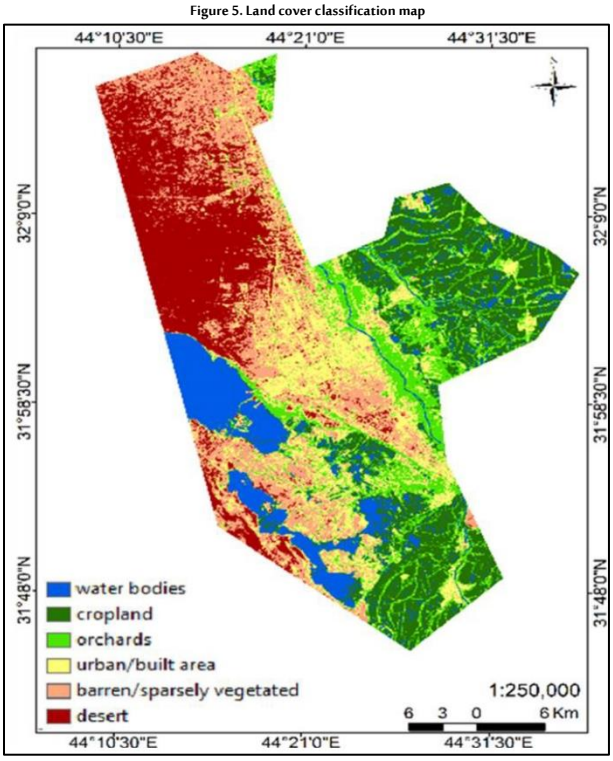

6. Conclusion

The observed desertification indicator was proposed according to the relationship between desertification and a combination of several indices: TCW-TCB, TCG-TCB, MSAVI-GSI and MSAVI-albedo. The proposed indices were used to evaluate desertification in a part of An-Najaf Province utilising Landsat 8 OLI imagery.

The results of the study show that degrees of desertification can be inferred using the feature-space models of TCG-TCB and TCW-TCB, where results manifested the highest negative correlation giving better results compared with MSAVI-albedo and MSAVI-GSI combined with p values of accuracy less than 0.0001. According to the relationship between TCG-TCB and TCW-TCB, the DDI has been applied for mapping the degree of desertification. The obtained values were, then, classified into five grades of desertification: none, low, medium, high and severe.

It was found that both models, TCW-TCB and TCG-TCB, presented a good result for assessing the degree of desertification with an overall accuracy of 88.14% and 91.44%, respectively. Therefore, it can be concluded that the calculation of the DDI index makes it possible to easily monitor desertification and effectively use remote sensing images from other sensors. Furthermore, the approach used is rapid and simple for quantitative evaluation of land degradation.

Biographies

Reem Tuama Yousuf

Department of Physics, College of Education for Girls, University of Kufa, Kufa, Iraq, 0096407816052719, reem94tooma@gmail.com

Mrs Yousuf holds a Bachelor of Science in physics from the University of Babylon. She is currently a master's student in remote sensing physics at the University of Kufa, College of Education for Girls. She has previously published an ISI/Scopus-indexed article in the field of remote sensing in the Journal of Xidian University. She is preparing to discuss her master's thesis, entitled 'Quantitative evaluation of desertification manifestation of a part of Najaf province using remote sensing data and spectral indexes techniques'.

Ebtihal T AL-Khakani

Department of Physics, College of Education for Girls, University of Kufa, Kufa, Iraq, 0096407829785431, ibtihal.alkhaqani@uokufa.edu.iq

Dr AL-Khakani is an assistant professor specialising in remote sensing physics who has participated in many international scientific conferences inside Iraq, published eight research papers in refereed journals in Iraq, and has publishing in journals with an international scope such as *Ecology, Environment and Conservation* and *Journal of Physics*. Dr AL-Khakani's main research interests are the use of remote sensing techniques in environmental monitoring, detection of change in land surface cover, soil salinity estimation, heat island measurement, and detection of surface soil minerals. ORCID: 0000-0002-4003-0154

References

Al-Bakri, J., Saoub, H., Nickling, W., Suleiman, A., Salahat, M., Khresat, S. and Kandakj, T. (2012). Remote sensing indices for monitoring land degradation in a semiarid to arid basin in Jordan. In: *Proc. SPIE 8538, Earth Resources and Environmental Remote Sensing/GIS Applications III, 853810*, Edinburgh, United Kingdom, 25/10/2012. doi: 10.1117/12.974333.

AL-Khakani, E.T., Al-Janabi, W.F., Yousif, S.R. and Al-Kazaali, H.M. (2018). Using Landsat 8 OLI data to predict and mapping soil salinity for part of An-Najaf governorate. *Ecology, Environment and Conservation*, **24**(2), 572–8.

AL-Khakani, E.T. and Yousif, S.R. (2019). An assessment of soil salinity and vegetation cover changes for a part of An-Najaf governorate using remote sensing data. In: *The 1st International Scientific Conference on Pure Science*, Al-Qadisiyah University, Al-Qadisiyah, Iraq, 23-24/1/2019.

An, H., Tang, Z., Keesstra, S. and Shangguan, Z. (2019). Impact of desertification on soil and plant nutrient stoichiometry in a desert grassland. *Scientific Reports*, **9**(9422), 1–9. DOI: 10.1038/s41598-019-45927-0.

Balcik, F.B. and Ergene, E.M. (2016). Determining the impacts of land cover/use categories on land surface temperature using Landsat 8-OLI. In: *XXIII ISPRS Congress*, Prague, Czech Republic, 12–19/07/2016. DOI: 10.5194/isprsarchives-XLI-B8-251-2016.

Baraldi, A., Puzzolo, V., Blonda, P., Bruzzone, L. and Tarantino C. (2006). Automatic spectral rule-based preliminary mapping of calibrated Landsat TM and ETM+ images. *IEEE Transactions on Geoscience and Remote Sensing*, **44**(9), 2563–86.

Becerril-Pina, R., Diaz-Delgado, C., Mastachi-Loza, C.A. and González-Sosa, E. (2016). Integration of remote sensing techniques for monitoring desertification in Mexico. *Human and Ecological Risk Assessment: an International Journal*, **22**(6), 1323–40. DOI 10.1080/10807039.2016.1169914.

Briassoulis, H. (2019). Combating land degradation and desertification: The land-use planning quandary. *Land*, **8**(27), 1–26. DOI: 10.3390/land8020027.

Crist, E.P. and Kauth, R.J. (1986). The tasseled cap de-mystified. *Photogrammetric Engineering and Remote Sensing*, **52**(1), 81–6.

Guangyin, H.U., Zhibao, D., and Junfeng, L.U. (2015). The developmental trend and influencing factors of aeolian desertification in the Zoige Basin, eastern Qinghai–Tibet Plateau. *Aeolian Research*, **19**(n/a), 275–81. DOI: 10.1016/j.aeolia.2015.02.002.

Cui, G., Lee, W.K., Kwak, D. A., Choi, S., Park T. and Lee, J. (2011). Desertification monitoring by LANDSAT TM satellite imagery. *Forest Science and Technology*, **7**(3), 110–6. DOI: 10.1080/21580103.2011.594607.

Guo, Q., Fu, B., Shi, P., Cudahy, T., Zhang, J. and Xu, H. (2017). Satellite monitoring the spatial-temporal dynamics of desertification in response to climate change and human activities across the Ordos Plateau, China. *Remote Sensing*, **9**(525), 1–20. DOI: 10.3390/rs9060525.

Huang, C., Wylie, B., Yang, L., Homer, C. and Zylstra, G. (2002). Derivation of a tasselled cap transformation based on Landsat 7 at-satellite reflectance. *International Journal of Remote Sensing*, **23**(8), 1741–8. DOI: 10.1080/01431160110106113.

Kauth, R.J. and Thomas, G.S. (1976). The tasselled cap – a graphic description of the spectral-temporal development of agricultural crops as seen by Landsat, In: *Proceedings of the Symposium on Machine Processing of Remotely Sensed Data*, Purdue University of West Lafayette, Indiana, 29/06–1/07/1976.

Lamqadem, A.A., Saber, H. and Pradhan, B. (2018a). Quantitative assessment of desertification in an arid oasis using remote sensing data and spectral index techniques. *Remote Sensing*, **10**(1862), 1–19. DOI:10.3390/rs10121862.

Lamqadem, A.A., Pradhan. B., Saber, H. and Rahimi, A. (2018b). Desertification sensitivity analysis using MEDALUS model and GIS: A case study of the oases of middle Draa Valley, Morocco. *Sensors*, **18**(7), 1–19. DOI: 10.3390/s18072230.

Liang, S.L. (2001). Narrowband to broadband conversions of land surface albedo I: Algorithm. *Remote Sensing Environment*, **76**(2), 213–38. DOI: 10.1016/S0034-4257(00)00205-4.

Li, B., Ti, C., Zhao, Y. and Yan, X. (2016). Estimating soil moisture with Landsat data and its application in extracting the spatial distribution of winter flooded paddies. *Remote Sensing*, **8**(38), 1–18. DOI: 10.3390/rs8010038.

Li, S. and Chen, X. (2014) A new bare-soil index for rapid mapping developing areas using Landsat 8 data. In: *The International Archives of the Photogrammetry, Remote Sensing and Spatial Information Sciences*, Suzhou, China, 14–16/5/2014. DOI: 10.5194/isprsarchives-XL-4-139-2014.

Ma, Z., Xie, Y., Jiao, J., li, L. and Wang, X. (2011). The construction and application of an Albedo-NDVI based desertification monitoring model. *Procedia Environmental Sciences*, **10**(n/a), 2029–35.

Mfondoum, A.H.N., Etouna, J., Nongsi, B. K., MvogoMoto. F.A. and Deussieu, F. G. N. (2016). Assessment of land degradation status and its impact in arid and semi-arid areas by correlating spectral and principal component analysis Neo-bands. *International Journal of Advanced Remote Sensing and GIS*, **5**(2), 1539–60.

Pandey, P. Ch., Rani, M., Srivastava, P.K., Sharma, L.K. and Nathawat, M.S. (2013). Land degradation severity assessment with sand encroachment in an ecologically fragile arid environment: A geospatial perspective. *QScience Connect*, **43**(n/a), 1–17. DOI: 10.5339/connect.2013.43.

Perry, C. J. and Lautenschlager, L.F. (1984). Functional equivalence of spectral vegetation indices. *Remote Sensing of Environment*, **14**(1-3), 169–82.

Röder, A. and Hill, J. (2008). Trend analysis of Landsat-TM and -ETM+ imagery to monitor grazing impact in a rangeland ecosystem in northern Greece. *Remote Sens Environ*, **112**(6), 2863–75.

Samarawickrama, U., Piyaratne1, D. and Ranagalage, M. (2017). Relationship between NDVI with tasseled cap indices: A remote sensing-based analysis. *International Journal of Innovative Research in Technology*, **3**(12), 13–9.

UNCCD. (1994). *United Nations Convention to Combat Desertification in those Countries Experiencing Serious Drought and/or Desertification, Particularly in Africa*. Paris, France, 19/06/1994.

Verstraete, M.M. and Pinty, B. (1996). Designing optimal spectral indexes for remote sensing applications. *Remote Sensing of Environment*, **34**(5), 1254–65.

Wang, G.J. and Zhang, J.C. (2007). Analysis of grassland desertification due to coal mining based on remote sensing - An example from huolinhe open-cast coal mine. *Journal of China University of Mining and Technology*, **10**(6), 917–25.

Wei, H., Wang, J., Cheng, K., Li, G., Ochir A., Davaasuren, D. and Chonokhuu, S. (2018). Desertification information extraction based on feature space combinations on the Mongolian plateau. *Remote Sensing*, **10**(10), 1614. DOI: 10.3390/rs10101614.

Wu, Z., Lel, Sh., Bian, Z., Huang, J. and Zhang, Y. (2019). Study of the desertification index based on the albedo-MSAVI feature space for semi-arid steppe region. *Environmental Earth Sciences*, **78**(232), 1–13. DOI: 10.1007/s12665-019-8111-9.

Xiao, J., Shen, Y., Tateishi, R. and Bayaer, W. (2006). Development of topsoil grain size index for monitoring desertification in arid land using remote sensing. *International Journal of Remote Sensing*, **27**(12), 2411–22. DOI: 10.1080/01431160600554363.

Xu, D., Kang, X., Qiu, D., Zhuang, D. and Pan, J. (2009). Quantitative assessment of desertification using Landsat data on a regional scale – A case study in the Ordos Plateau, China. *Sensors*, **9**(3), 1738–53. DOI: 10.3390/s90301738.

Xu, D. and Ding, X. (2018). Assessing the impact of desertification dynamics on regional ecosystem service value in North China from 1981 to 2010. *Ecosystem Services*, **30**(n/a), 172–80. DOI: 10.1016/j.ecoser.2018.03.002.

Zanchetta, A. and Bitelli, G. (2017). A combined change detection procedure to study desertification using open source tools. *Open Geospatial Data, Software and Standards*, **2**(10), 1–12. DOI: 10.1186/s40965-017-0023-6.